Automatic Through the Wall Detection of Moving Targets using Low-Frequency Ultra-Wideband Radar

Anthony Martone, Kenneth Ranney,
and Roberto Innocenti
Army Research Laboratory, 2800 Powder Mill Rd
Adelphi, MD 20783 USA

Abstract— **This paper presents a time-domain, Moving Target Indication (MTI) processing formulation for detecting slow-moving personnel behind walls. The proposed time-domain MTI processing formulation consists of change detection and automatic target recognition algorithms. We demonstrate the effectiveness of the MTI processing formulation using data collected by an impulse-based, low-frequency, ultra-wideband radar. In this paper, we describe our radar system and algorithms used for the automatic detection of moving personnel. We also analyze the false alarm and detection rate of four operational scenarios of personnel walking inside wood and cinderblock buildings.**

I. INTRODUCTION

Current and future forces operating in urban environments need the capability to detect slow-moving personnel inside buildings. To identify moving personnel inside buildings, we consider a time-domain approach that utilizes a low-frequency, ultra-wideband (UWB) radar. A low-frequency, UWB radar is desired since the low-frequency transmit pulse is capable of penetrating the wall [1] and the ultra-wide bandwidth produces the high range resolution necessary to locate the moving target.

We consider a time-domain approach to moving target indication (MTI) as an alternative to a frequency-domain approach, i.e. Doppler processing, since a very small Doppler shift in backscattered frequency is generated due to: 1) the slow motion of the mover and 2) the low frequency needed to penetrate through the wall. Our time domain processing algorithms are based on the change detection paradigm which is inherently similar to clutter cancellation [2]. In the change detection paradigm the radar remains stationary and generates a set of images for a region of interest (ROI). Each image in the set is formed every two-thirds of a second. The stationary objects in the building remain in the same position/location in each radar image; however, moving personnel will be at different locations. We can therefore detect the moving personnel by subtracting adjacent radar images in the set, thereby eliminating the stationary objects and identifying the moving target (MT) signature.

Our previous research [3] discusses multiple scenarios of people walking inside wood and cinderblock structures, and walking in linear and non-linear trajectories (notice that all results are based on experimental data, not on simulations). In all scenarios the slow-moving personnel were detected using the change detection paradigm.

Interpretation of the resulting MT signature, however, is still challenging after change detection. For example, due to false-alarm artifacts, previous results [3] indicate that change detection cannot automatically identify the moving target located in the difference image. The moving target can only be identified through visual inspection of the difference image. Therefore, it is not possible to implement additional signal processing techniques like classification or target tracking. Another challenge with change detection is that sidelobe artifacts are produced in the difference image, which confuse the true moving target location.

A way to improve user interpretation of the resulting difference image is to apply the constant false alarm rate (CFAR) algorithm [4] and morphological processing [5]. CFAR is an approach used to eliminate imaging artifacts and potential false alarms associated with the slow-moving targets (e.g. low-intensity ("faint") target responses due to multi-path effects). The morphological processing is used to further reduce the potential false alarms in the CFAR output image. In this paper, we will use these techniques to analyze the false alarm and detection rates of 4 operational scenarios of personnel walking inside wood and cinderblock buildings.

II. SYNCHRONOUS IMPULSE RECONSTRUCTION RADAR

The U.S. Army Research Laboratory (ARL) has developed a ground-based Synchronous Impulse Reconstruction (SIRE) radar [6] to aid in the detection of concealed targets [7]. The SIRE radar is an impulse-based, UWB imaging radar with a bandwidth covering 300MHz to 3GHz, a frequency range appropriate for sensing through the wall (STTW) applications [1]. As is illustrated in Figure 1, the SIRE radar employs 2 transmit antennas and 16 receiver antennas mounted in a wooden frame and attached to the top of a Ford Expedition. The receive antennas are equally spaced across a linear aperture that is 2m long. The two impulse transmitters are located at each end of the wooden frame and slightly above the receive array. The SIRE radar constructs a high-resolution (0.15m) down-range profile through novel, ARL-developed signal-processing techniques [7].

Report Documentation Page

1. REPORT DATE **MAY 2010**	2. REPORT TYPE	3. DATES COVERED **00-00-2010 to 00-00-2010**

4. TITLE AND SUBTITLE **Automatic Through the Wall Detection of Moving Targets using Low-Frequency Ultra-Wideband Radar**		5a. CONTRACT NUMBER
		5b. GRANT NUMBER
		5c. PROGRAM ELEMENT NUMBER
6. AUTHOR(S)		5d. PROJECT NUMBER
		5e. TASK NUMBER
		5f. WORK UNIT NUMBER

7. PERFORMING ORGANIZATION NAME(S) AND ADDRESS(ES) **Army Research Laboratory,2800 Powder Mill Rd,Adelphi,MD,20783**	8. PERFORMING ORGANIZATION REPORT NUMBER
9. SPONSORING/MONITORING AGENCY NAME(S) AND ADDRESS(ES)	10. SPONSOR/MONITOR'S ACRONYM(S)
	11. SPONSOR/MONITOR'S REPORT NUMBER(S)

12. DISTRIBUTION/AVAILABILITY STATEMENT
Approved for public release; distribution unlimited

13. SUPPLEMENTARY NOTES
See also ADM002322. Presented at the 2010 IEEE International Radar Conference (9th) Held in Arlington, Virginia on 10-14 May 2010. Sponsored in part by the Navy.

14. ABSTRACT
This paper presents a time-domain, Moving Target Indication (MTI) processing formulation for detecting slowmoving personnel behind walls. The proposed time-domain MTI processing formulation consists of change detection and automatic target recognition algorithms. We demonstrate the effectiveness of the MTI processing formulation using data collected by an impulse-based, low-frequency, ultra-wideband radar. In this paper, we describe our radar system and algorithms used for the automatic detection of moving personnel. We also analyze the false alarm and detection rate of four operational scenarios of personnel walking inside wood and cinderblock buildings.

15. SUBJECT TERMS

16. SECURITY CLASSIFICATION OF:			17. LIMITATION OF ABSTRACT	18. NUMBER OF PAGES	19a. NAME OF RESPONSIBLE PERSON
a. REPORT **unclassified**	b. ABSTRACT **unclassified**	c. THIS PAGE **unclassified**	**Same as Report (SAR)**	**5**	

(a) Forward-looking configuration.　　**(b) Side-looking configuration.**
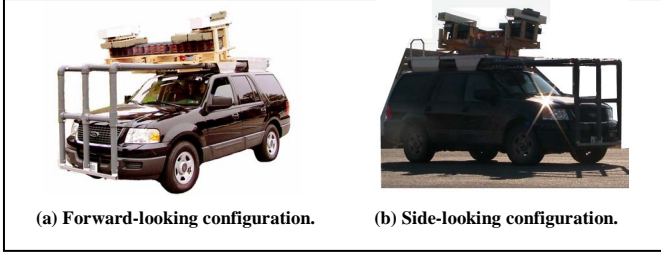
Figure 1: The SIRE Radar.

III.　APPROACH TO MOVING TARGET INDICATION

Our approach to MTI consists of change detection, CFAR processing, and morphological processing. The SIRE radar remains stationary and measures the energy reflected from a ROI. We begin the MTI processing by buffering downrange profiles measured by each receive channel for a single pair of transmit pulses. Since the transmitters fire in sequence—the left transmitter followed by the right transmitter—we effectively buffer two downrange profiles from each receive channel, and the time required to assemble these profiles represents one frame of data. After buffering the data from one frame, we then collect another pair of downrange profiles from each receive channel for the next frame of data. Finally, we form the coherent difference between these newly collected profiles and the corresponding buffered profiles to obtain a new data set consisting of modified downrange profiles defined by

$$\dot{f}_{i,j,k}(r) = f_{i+1,j,k}(r) - f_{i,j,k}(r) \qquad (1)$$

where $i = 1,...,N-1$, $j = 1,2$, and $k = 1,...,16$. Here r represents the downrange index, i represents the slow-time (frame) index, j represents the transmitter index, and k represents the receiver index. Hence, we are forming a signal that monitors changes between the two sets of downrange profiles measured at time i and time $i+1$ using transmitter j and receiver k. This is why we refer to our model as a "change detection" (CD) paradigm. The difference signal, $\dot{f}_{i,j,k}(r)$ (corresponding to the derivative in time), is then input to an image formation routine, in our case a time-domain back-projection procedure [8], resulting in the set difference images:

$$I_i(x,y) = \sum_{k=1}^{16}\sum_{j=1}^{2} g(i,j,k)\dot{f}_{i,j,k}(r_{x,y}(j,k)) \qquad (2)$$

where $g(i,j,k)$ is a scaling function, $x = 1,...500$, $y = 1,...500$, and $r_{x,y}(j,k)$ is the round-trip distance from transmitter j to pixel (x,y) and back to receiver k.

A way to improve user interpretation of the resulting difference image is to apply a constant false alarm rate (CFAR) algorithm. CFAR is a well-established approach to eliminating potential false alarms. Typically, the algorithm performs a test of local contrast that is designed to achieve a constant false alarm rate [4]. For a given difference image $I_i(x,y)$, a CFAR window is used to scan the difference image and test for the MT signature.

As illustrated in Figure 2, the CFAR window contains an inner window, a guard window, and an outer window. The inner window dimensions are designed so that it is overlaid on the MT signature. When the inner window is overlaid on the MT signature, the outer window dimensions are designed to be superimposed on the local background. The guard window is used as a buffer between the inner and outer windows and ensures that large pixel magnitudes due to target sidelobes are not captured by the outer window. Based on our observations and analysis of the MT signatures, we have chosen the inner window to be (0.36x0.28)m or (9x7)pixels, the guard window to be (0.92x1)m or (23x25)pixels, and the outer window to be (1.16x1.08)m or (29x27)pixels, where the parentheses denote (range x cross-range) dimensions.
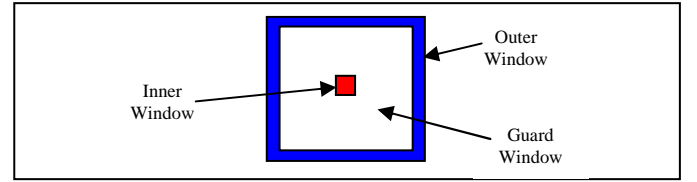

Figure 2: CFAR Window.

The CFAR window is placed in the difference image and moved pixel by pixel over the entire difference image. The CFAR algorithm indicates a point of interest (POI) if the sum of the energy in the inner window is larger than the sum of the energy in the outer window. For any given location in the difference image, the inner window to outer window energy ratio is defined as

$$R = \frac{\mu_i}{\mu_o} \qquad (3)$$

where $\mu_i = \sum_{(l,k)\in\gamma_i}[\Phi(P_{l,k})^2]$ is the sum of the power the inner window, $\mu_o = \sum_{(m,n)\in\gamma_o}\Phi[(P_{m,n})^2]$ is the sum of the power in the outer window, $P_{l,k}$ is the magnitude of the pixel at position (l,k) in the difference image, γ_i is the set of pixels in the inner window, and γ_o is the set of pixels in the outer window. Define

$$\Phi(P_{l,k}) = \begin{cases} P_{l,k}, & P_{l,k} > \eta \\ \eta, & P_{l,k} \le \eta \end{cases}, \qquad (4)$$

where $\eta = \max(P_{l,k})$ and $\max(P_{l,k})$ is the maximum pixel magnitude in the difference image. The function $\Phi(P_{l,k})$ is used to adjust the image background and requires that the magnitude of each pixel is above the threshold defined by η, which is done to prevent errors due to division by very small numbers. Division by very small numbers artificially inflates the ratio defined by equation (3) and causes false positives. The threshold η was chosen based on the observations of the

sidelobes corresponding to the MT signature, which are typically less than $\max(P_{l,k})/2$ in magnitude. This choice of η eliminates the sidelobes by blending them into the background of the difference image. Define a CFAR test as

$$\Psi_c = \begin{cases} 1 & R > T \\ 0 & else \end{cases}, \qquad (5)$$

This test requires that the sum of the energy in the inner window is greater than T times the sum of the energy in the outer window, where $T = 2$. If $\Psi_c = 1$, then the center pixel of the CFAR window is considered as a POI. The POI corresponds to either a moving target or a false alarm. The CFAR algorithm generates a CFAR image, $C_i(x, y)$, for each input difference image $I_i(x, y)$. $C_i(x, y)$ contains clusters of POIs corresponding to either the MT signature or false alarms. Note that $C_i(x, y) = 1$ or $C_i(x, y) = 0$ $\forall$ i, x, y, meaning that the pixels in the CFAR images are binary.

We next apply morphological processing to further refine the number of clusters present in the CFAR images. The morphological processing considered implements a dilation and erosion procedure [5]. Dilation is used to grow the POI clusters and erosion is used to shrink the POI clusters. The dilation process is designed to connect clusters in close proximity by dilating all pixels in each CFAR image. For dilation we define a 17x17 dilation window χ_d:

$$[\chi_d]_{17,17} = \begin{bmatrix} 1 & \cdots & 1 \\ \vdots & \ddots & \vdots \\ 1 & \cdots & 1 \end{bmatrix}$$

The 17x17 dilation window size was chosen to connect clusters separated by a distance of 0.68m or less (this distance was chosen based on observations of the clusters in the CFAR images). Similar to CFAR, a dilation test statistic is defined:

$$\Psi_d = \begin{cases} 1, & \sum_{\alpha=1}^{17}\sum_{\beta=1}^{17} \chi_d(\alpha,\beta) \cdot C_i(j+\alpha-1, k+\beta-1) > 0 \\ 0, & else \end{cases} \quad (6)$$

for all $j = 1,...484$ and $k = 1,...484$. When the dilation window scans the CFAR image, an 8 pixel buffer exists along the edge of the CFAR image (i.e. not enough samples exist at the edges of the image). There exist $i = 1,...N-1$ dilation images; one for each CFAR image. If $\Psi_d = 1$ for a given i, j, k then a dilation occurs and $D_i(j+8, k+8) = 1$, where $D_i(x, y)$ is a dilation image of size (500x500). If $\Psi_d = 0$, then $D_i(j+8, k+8) = 0$, and no dilation occurs.

We next apply an erosion procedure to reduce the size of the clusters in the dilation image back to their original size in the CFAR image. Any clusters joined using the dilation

process will remain joined after the erosion process. For erosion we define a 17x17 erosion window χ_e:

$$[\chi_e]_{17,17} = \begin{bmatrix} 0 & \cdots & 0 & 1 & 0 & \cdots & 0 \\ \vdots & \ddots & \vdots & \vdots & \vdots & \ddots & \vdots \\ 0 & \cdots & 0 & \vdots & 0 & \cdots & 0 \\ 1 & \cdots & \cdots & 1 & \cdots & \cdots & 1 \\ 0 & \cdots & 0 & \vdots & 0 & \cdots & 0 \\ \vdots & \ddots & \vdots & \vdots & \vdots & \ddots & \vdots \\ 0 & \cdots & 0 & 1 & 0 & \cdots & 0 \end{bmatrix}$$

Similar to the dilation procedure, we define the erosion test statistic as

$$\Psi_e = \begin{cases} 1 & \gamma = \Omega \\ 0 & else \end{cases} \qquad (7)$$

where

$$\gamma = \sum_{\alpha=1}^{17} \chi_e(\alpha,9) \cdot D_i(j+\alpha-1, k+8)$$
$$+ \sum_{\beta=1}^{17} \chi_e(9,\beta) \cdot D_i(j+8, k+\beta-1),$$

$\Omega = 34$ is the erosion threshold, $j = 1,...484$, and $k = 1,...484$. There exist $i = 1,...N-1$ erosion images; one for each dilation image. If $\Psi_e = 1$ for a given i, j, k, then $E_i(j+8, k+8) = 1$, where $E_i(x, y)$ is an erosion image of size (500x500). If $\Psi_e = 0$, then an erosion occurs and $E_i(j+8, k+8) = 0$. We refer to the set of erosion images, $\{E_1(x, y)...E_{N-1}(x, y)\}$, as the morphological output images.

IV. EXPERIMENTAL RESULTS

In previous experimentation, data was collected for multiple scenarios of personnel walking inside wood and cinderblock buildings [3]. During the collection of the data, the SIRE radar remained stationary and was positioned broadside to the wall and 38° off the broadside position. The off-broadside angle was selected in an attempt to reduce imaging artifacts present in the difference images due to large reflections from the wall. The measured data was processed using the proposed change detection technique. The results of this experimentation indicated that the MT signature to wall noise ratio in the difference images was reduced when imaging inside the wood building (compared to cinderblock building) at 38° off the broadside position.

In this paper, we will consider a subset of the same data and scenarios described in [3]. For all scenarios, our radar

collected 35 frames of data. The proposed approach described in Section III was used to process 35 frames for each scenario. Scenario 1 consists of a person walking in a circular pattern inside a wood building where the radar is positioned broadside to the wall. Key morphological images, or key frames, are shown in Figure 3 for Scenario 1, where the key frames indicate different instants in time. For all scenarios, the key frames presented represent only a subset of all morphological images available. As illustrated, the clusters in each key frame represent the MT signature. As shown, no imaging artifacts are present in the key frames (or any other morphological image for this scenario). Frame 1 is a morphological image of the person moving away from the radar ("2 O'clock" position on the circular trajectory), Frame 2 is an image of the person moving away from the radar ("5 O'clock" position on the circular trajectory), and Frame 3 is an image of the person moving toward the radar ("10 O'clock" position on the circular trajectory).
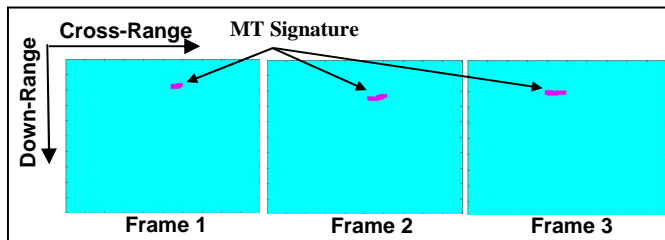

Figure 3: Key frames of the morphological output images for Scenario 1. The person is walking in a circular pattern inside the wood building and the radar is positioned broadside with respect to the wall.

Scenario 2 consists of a person walking in a circular pattern inside a wood building where the radar is positioned 38˚ off the broadside position. Key frames are shown in Figure 4 for Scenario 2. The MT Signature is present in all key frames and they are larger than the MT signatures illustrated in Scenario 1. The increased size of the MT signature corresponds to additional uncertainty regarding the moving target's location. In addition to the increase in MT signature size, false alarms are present in the morphological images as indicated by key frame 2 in Figure 4.
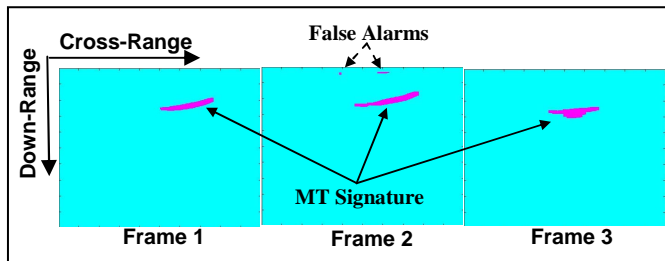

Figure 4: Key frames of the morphological output images for Scenario 2. The person is walking in a circular pattern inside the wood building and the radar is positioned 38˚ off the broadside angle.

Scenario 3 consists of a single person walking along a random trajectory inside the cinderblock building, and the radar is positioned broadside with respect to the wall. Key frames for Scenario 3 are shown in Figure 5. Similar to Scenario 2, false alarms are present in the key frames. However, unlike Scenarios 1 and 2, the MT signature is not present in all key frames.
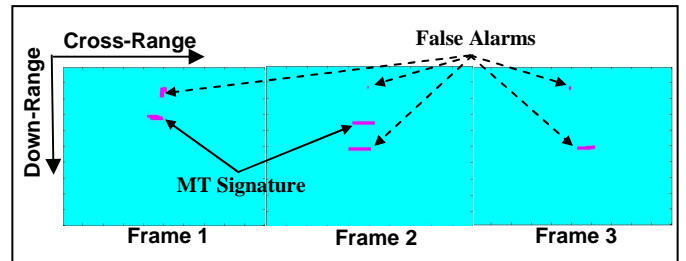

Figure 5: Key frames of the morphological output images for Scenario 3. The person is walking randomly inside the cinderblock building and the radar is positioned broadside to the wall.

Scenario 4 consists of a single person walking along a random trajectory inside the cinderblock building, and the radar is positioned 38˚ off the broadside angle. Key frames for Scenario 4 are shown in Figure 6. The MT signature is illustrated in the key frames and all other clusters are false alarms. The three notable observations of the clusters present in the key frames of Scenario 4 are: (i) several false alarms are present, (ii) the MT signatures are preserved, and (iii) the size of the MT signature is very large.
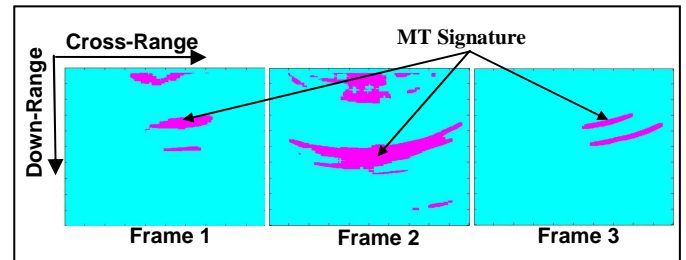

Figure 6: Key frames of the morphological output images for Scenario 4. The person is walking randomly inside the cinderblock building and the radar is positioned 38 degrees off the broadside angle.

We analyzed the clusters in all morphological images for each scenario. This analysis consisted of examining: N - the total number frames, N_c - the total number of clusters, N_{fa} - the number of false alarms, N_d - the number of moving target detections, N_μ - the average number of pixels in the MT signature, $P_{fa} = (N_{fa} / N_c)$ - the probability of false alarm, and $P_d = N_d / N$ - the probability of detection. The results are illustrated in Table 1.

Table 1: Statistics of morphological images for each scenario.

Scenario	N	N_c	N_{fa}	N_d	P_{fa}	P_d	N_μ
1	35	35	0	35	0	1	464.9
2	35	54	19	35	0.35	1	1596
3	35	47	36	11	0.77	0.31	520
4	35	196	161	35	0.82	1	4195

As is shown in Table 1, imaging inside a wood building when the radar is broadside to the wall (Scenario 1) is the most favorable scenario, which is evident by $P_{fa}=0$ and $P_d=1$. Imaging the wood building at an off angle (Scenario 2) increases the false alarm rate and average number of pixels in the MT signature. The false alarms are generated when their energy is of the same magnitude as the energy of the MT signature. This effect is the result of imaging at an off angle

and is due to the energy scattering effects from the wall and building geometry.

The cinderblock wall in Scenario 3 absorbs and scatters more energy from the transmit waveform than does the wood wall in Scenarios 1 and 2. The energy of the MT signature is therefore severely attenuated, and the magnitude of the front wall signature is the same or greater than that of the moving person. Hence, the front wall in the difference image is not effectively canceled by change detection [3], and the CFAR algorithm preserves false alarms and reduces the MT signature. This fact is evident by examining P_d and P_{fa}. P_d indicates that the MT signature is only present in 31% of the morphological images and P_{fa} indicates that 77% of all clusters are false alarms.

Unlike Scenario 3, the MT signature is preserved in every morphological image of Scenario 4 and is evident by $P_d=1$. However, the number of false alarms for Scenario 4, i.e. $N_\alpha=196$, is significantly higher than any other scenario. In addition, the average number of pixels in the MT signature, $N_\mu=4195$, is greatly increased. In this scenario, the energy of the MT signature is attenuated by absorption of the cinderblock wall (as described in Scenario 3) and imaging at an off angle (as described in Scenario 2). The CFAR algorithm, therefore, preserves the false alarms in addition to the MT signature. Furthermore, the morphological processing algorithm will merge false alarms with the MT signature resulting in a larger than expected MT signature. An example of this effect is shown by key frame 2 in Figure 6, where the large cluster is a result of the true MT signature and several merged false alarms.

V. CONCLUSION

We demonstrated the effectiveness of our time-domain MTI processing technique for automatically detecting moving personnel walking in non-linear trajectories inside both wood and cinderblock building structures. The results indicated that imaging inside a wood building when the radar is broadside to the wall (Scenario 1) is the most favorable scenario with $P_{fa}=0$ and $P_d =1$. When the radar was positioned 38˚ off the broadside angle for the wood wall (Scenario 2), detection performance was $P_d =1$. However, an increase in false alarm rate was produced, and this increase was due to the energy scattering and multipath effects encountered when imaging at an off angle.

Sensing through a cinderblock wall when the radar was positioned broadside to the wall (Scenario 3) produced missed detections of the MT signature and false alarms—effects due to the energy scattering/absorption effects of the cinderblock

wall. Sensing through a cinderblock wall when the radar was at an off broadside angle (Scenario 4) produced no missed detections while yielding the largest number of false alarms. This performance was most likely due to the energy-scattering and multipath effects of the cinderblock wall encountered when imaging at an off angle.

Our results indicate the feasibility of detecting moving personnel inside wood buildings. Detecting moving personnel inside cinderblock buildings, however, is more challenging. As part of future research efforts, we will consider techniques to eliminate the large energy response produced by the cinderblock wall, and we will evaluate techniques for eliminating false alarms. We also plan to examine the false alarms produced by multipath effects by modeling each of the 4 scenarios described in this paper.

REFERENCES

[1] M. Farwell, J. Ross, R. Luttrell, D. Cohen, W. Chin, and T. Dogaru, "Sense through the wall system development and design considerations," *Journal of the Franklin Institute,* vol. 345, no. 6, September 2008, pp. 570-591.

[2] L. Novak, "Change detection for multi-polarization, multi-pass SAR," *in Proceedings of the SPIE Conference on Algorithms for Synthetic Aperture Radar Imagery XII*, vol. 5808, Orlando, FL, March 2005, pp. 234-246.

[3] A. Martone, K. Ranney, R. Innocenti, "Through the wall detection of slow moving personnel," *in Proceedings of the SPIE conference on Radar Sensor Technology XIII*, vol. 7308, Orlando, Fl, April 2009.

[4] P. Gandhi, and S. Kassam, "Analysis of CFAR processors in homogeneous background," *IEEE transactions on Aerospace and Electronic Systems*, vol. 24, no. 4, July 1988.

[5] A. Jain, *Fundamentals of Digital Image Processing*. Prentice-Hall International, Englewood Cliffs, NJ, 1989.

[6] M. Ressler, L. Nguyen, F. Koenig, D. Wong, D, G. Smith, "The Army Research Laboratory (ARL) Synchronous Impulse Reconstruction (SIRE) Forward-Looking Radar," *in Proceedings of the SPIE Conference on Unmanned Systems Technology IX,* vol. 6561, Bellingham, Wa, April 2007, pp. 656105-1 – 656105-12.

[7] J. McCorkle, "Focusing of Synthetic Aperture Ultra Wideband Data," *in Proceedings of the IEEE International Conference on Systems Engineering*, Dayton, Oh, August 1991, pp. 1-5.

[8] Nguyen, L. *Image Resolution Computation for Ultra-Wideband (UWB) Synchronous Impulse Reconstruction (SIRE) Radar*; ARL-TN-0294; U.S. Army Research Laboratory: Adelphi, MD, July 2007.